Covariance Cost Functions for Scheduling Multistatic Sonobuoy Fields

Christopher Gilliam[1], Daniel Angley[2], Simon Williams[1], Branko Ristic[1], Bill Moran[2], Fiona Fletcher[3] and Sergey Simakov[3]

[1] School of Engineering, RMIT University, Australia

[2] Electrical & Electronic Engineering, University of Melbourne, Australia

[3] Maritime Division, Defence Science and Technology Group, Australia

***Abstract*—Sonobuoy fields, comprising a network of sonar transmitters and receivers, are used to find and track underwater targets. For a given environment and sonobuoy field layout, the performance of such a field depends on the scheduling, that is, deciding which source should transmit, and which waveform should be transmitted at any given time. In this paper, we explore the choice of cost function used in myopic scheduling and its effect on tracking performance. Specifically, we consider 5 different cost functions derived from the predicted error covariance matrix of the track. Importantly, our cost functions combine both positional and velocity covariance information to allow the scheduler to choose the optimum source-waveform action. Using realistic multistatic sonobuoy simulations, we demonstrate that each cost function results in a different choice of source-waveform actions, which in turn affects the performance of the scheduler. In particular, we show there is a trade-off between position and velocity error performance such that no one cost function is superior in both.**

***Index Terms*—Multistatic sonar; Sensor scheduling; Target tracking**

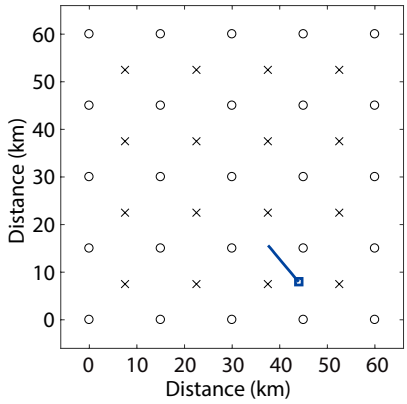

Fig. 1. Illustration of a multistatic sonobuoy field and a target. The crosses are transmitter sonobuoys and the circles are receivers. The blue line indicates the trajectory of the target and the square indicate its starting point.

I. Introduction

A multistatic sonobuoy field comprises a network of transmitters (sources) and receivers distributed across a large search area. The principal task of such a network is to search for and track underwater targets. The network operates by emitting an acoustic signal, or "ping", from a transmitter sonobuoy and receiving the signal, possibly reflected from a target, at nearby receivers. In our experiments, the ping can take the form of Doppler insensitive frequency modulated (FM) waveforms or Doppler sensitive continuous wave (CW) waveforms. FM waveforms provide target range and bearing measurements whereas CW waveforms provide target bearing, Doppler measurements and coarse range measurements. By fusing these measurements, the network of sensors is able to achieve high target detection performance in challenging underwater environments where the signal-to-noise ratio (SNR) of the returned signal is typically low and clutter is significant. An example of a sonobuoy field with 16 sources and 25 receivers is shown in Fig. 1. The blue line represents the trajectory of a target that the field must find and track.

Now, a key aspect in the performance of the sonobuoy field is the decision on which transmitter in the field should ping. The sequential order in which the sources in the network transmit, and which waveform they use, is governed by a central scheduler (i.e. sensor manager). Intelligent scheduling with the aim of improving the performance of a multistatic sonobuoy system was first proposed in [1]. The authors developed a framework for *greedy* (or myopic) scheduling with separate metrics for search and tracking. Since then significant work has been undertaken to define new metrics and greedy algorithms for scheduling. For example, search metrics based on the probability of undetected targets in the field have been investigated using diffusion concepts in [1], [2], Monto-Carlo techniques in [3], [4], and extended to incorporate target track information in [5]. Similarly, in terms of tracking, metrics based on weighting the track information were proposed in [6], and optimizing the expected number of target detections in [7]. More recently, a multi-objective framework for myopic scheduling was proposed in [8] whereby the search and track tasks were treated as competing objectives. A block diagram illustrating the role of the scheduler in a sonobuoy field is shown in Fig. 2. Note that *long term* (non-myopic) scheduling has also been investigated in [9]–[12].

In this paper, we examine the choice of tracking metrics used to schedule a multistatic sonobuoy field. More specifically, we focus on myopic scheduling for high-quality target tracking and explore cost functions based on the predicted

This research was supported in part by Defence Science and Technology Group under the Research Agreement "Enhanced Sensor Scheduling for Multistatic Sonar Systems".

future covariance matrix for the tracker (also known as the posterior Cramér-Rao bound [13]). The goal of our scheduler is thus to 'reduce' the covariance matrix by minimizing the cost functions. Such an approach has been used in sensor management problems [14]–[16] and in optimal waveform selection [17], [18]. These methods generally focus on using the positional information of the target state and computing the trace or determinant of the matrix [16]–[18], or they compare the predicted matrix to a desired minimum allowable covariance [14].

Instead, in this work, we consider the covariance matrix of the whole target state, including both position and velocity elements, and formulate 5 costs functions based on different ways of measuring the size of the hyper-ellipsoid it represents. In particular, along with the trace and determinant, we examine the maximum variance (i.e. maximum eigenvalue), the average precision (harmonic mean) and the joint maximum variance in both position and velocity as cost functions for scheduling. The advantage of using these functions is that they combine position and velocity accuracy into a single cost, which allows the scheduling to be posed as a single-objective minimization problem. An alternative method, not explored in this paper, would be to have separate cost functions for position and velocity, and use multi-objective optimization. Thus, instead of a single solution, there would be a frontier of solutions, which are Pareto optimal, describing the trade-off between position and velocity accuracy. Note that a similar approach was explored in [8] for the trade-off between tracking known targets and searching for unknown targets.

Using a realistic measurement simulation environment, we demonstrate that the choice of cost function affects which sources and waveforms are selected by the scheduler, which affects the tracking performance. We show that the performance of the cost functions are characterized by a trade-off between position and velocity accuracy; one cannot be improved without degrading the other. Thus, none of the cost functions considered can be thought of as superior to the others.

Note that the cost functions we discuss in this paper also arise as criteria in the optimal design of experiments [19]. For example, the trace, determinant and maximum variance costs are referred to as A-optimality, D-optimality and E-optimality, respectively.

The paper is organized as follows. In Section II, we review the main elements required for tracking in multistatic sonobuoy fields. In Section III, we present the framework of our scheduler and introduce five possible covariance-based cost functions that the scheduler can use when making its decision. We then analyze the performance of these criteria using simulations in Section IV. Finally we conclude in the last section.

II. Tracking in Multistatic Sonobuoy Fields

In this section, we review the main elements required to track a target in the sonobuoy field. Specifically, we cover the modelling of the sonobuoy field and targets; the type of measurements obtained from the receivers; the simulation environment used to generate realistic sonobuoy datasets; and the tracking algorithm.

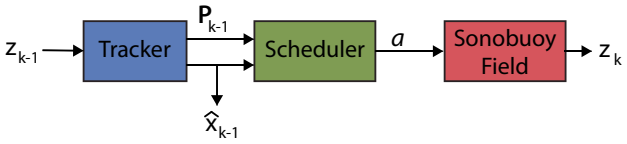

Fig. 2. Diagram illustrating the process of scheduling the multistatic sonobuoy field for target tracking. At time $k-1$, the tracker receives a set of measurements, $\mathbf{z}_{k-1}$, obtained from the sonobuoy field and outputs an estimate of the target's state $\hat{\mathbf{x}}_{k-1}$ and the associated error covariance $\mathbf{P}_{k-1}$. These quantities are then used by the scheduler to determine the next source to transmit in the field and which waveform to emit. This source-waveform pair, denoted a, results in the next set of measurements z_k.

A. Sonobuoy Field Geometry and Target Modelling

The multistatic sonobuoy field comprises a network of N_s sources and N_r receivers, see Fig. 1 for an illustration. The position of the jth source in the field is defined as $\mathbf{s}_j = \left[x_s^j, y_s^j\right]^{\mathrm{T}}$, where $j = 1, \ldots, N_s$ and the position of the ith receiver is defined as $\mathbf{r}_i = \left[x_r^i, y_r^i\right]^{\mathrm{T}}$, where $i = 1, \ldots, N_r$. These positions are assumed to be fixed for the duration of the simulation. In practice, this assumption is unlikely to be valid, due to effects such as ocean currents. However each buoy contains RF communications and may contain GPS equipment, so the position of the buoys can easily be tracked and accounted for in a practical deployment.

An underwater target within the field is described using the following time-varying state: $\mathbf{x}_k = [\mathbf{p}_k^{\mathrm{T}}, \mathbf{v}_k^{\mathrm{T}}]^{\mathrm{T}}$, where $\mathbf{p} = [x_k, y_k]^{\mathrm{T}}$ is the position of the target at time t_k and $\mathbf{v} = [\dot{x}_k, \dot{y}_k]^{\mathrm{T}}$ is its corresponding velocity. The motion of a target is approximated using a noisy linear constant-velocity model:

$$\mathbf{x}_k = f(\mathbf{x}_{k-1}) + \mathbf{e}_k = \left(\begin{bmatrix} 1 & T \\ 0 & 1 \end{bmatrix} \otimes \mathbf{I}_2 \right) \mathbf{x}_{k-1} + \mathbf{e}_k \qquad (1)$$

where $T = t_k - t_{k-1}$ is the sampling in time, $\mathbf{e}_k$ is the process noise, $\otimes$ is the Kronecker product and $\mathbf{I}_2$ is the 2×2 identity matrix. The process noise is Gaussian in nature and drawn from $\mathcal{N}(\mathbf{0}, \mathbf{Q})$, where the variance $\mathbf{Q}$ is defined as

$$\mathbf{Q} = \omega \begin{bmatrix} T^3/3 & T^2/2 \\ T^2/2 & T \end{bmatrix} \otimes \mathbf{I}_2$$

and ω is the intensity of the noise.

For this paper, we assume that the targets remain at a fixed depth when moving. The exact value of this depth is unknown to the tracker and scheduler; instead they are given knowledge of a maximum, $z_{\max}$, and minimum, $z_{\min}$, depth in which a target can occur.

B. Measurements Obtained from the Sonobuoy Field

Given the above geometric model, each source in the field has the ability to emit one of $N_w = 8$ waveforms; it can choose to emit either a FM or CW waveform, at a frequency of either 1kHz or 2kHz and with a transmission duration of either 2 or

8 seconds. When a source emits a waveform we obtain a set of measurements $\mathbf{Y}_k^{(i)}$ collected by a subset of the receivers $i \in I_k$, known as the proximal (or contributing) receivers. These measurements may relate to an actual target within the field or a phantom target created by a false detection.

Individually, a measurement $\mathbf{y} \in \mathbf{Y}_k^{(i)}$ comprises the kinematic measurement $\mathbf{z}$ and the returned signal amplitude β such that $\mathbf{y} = [\beta, \mathbf{z}^{\mathrm{T}}]^{\mathrm{T}}$. The components of the kinematic measurement $\mathbf{z}$ depend upon the type of waveform emitted by the source. If an FM waveform has been emitted, then $\mathbf{z}$ contains the bistatic range – the range from the source to the target to the receiver – and the angle from the receiver. In contrast, if a CW waveform has been used then, in addition to the bistatic range and the angle from the receiver, the vector $\mathbf{z}$ also includes the bistatic range-rate. Accordingly, for a waveform $\phi \in \{\mathrm{CW}, \mathrm{FM}\}$ and source j, we have:

$$\mathbf{z} = \mathbf{h}_{j,\phi}^{(i)}(\mathbf{x}_k) + \mathbf{w}_{j,\phi}^{(i)} \tag{2}$$

where $\mathbf{h}_{j,\mathrm{FM}}^{(i)}(\mathbf{x}_k) = \left[h_{j,\rho}^{(i)}(\mathbf{x}_k), h_{j,\theta}^{(i)}(\mathbf{x}_k)\right]^{\mathrm{T}}$ and $\mathbf{h}_{j,\mathrm{CW}}^{(i)}(\mathbf{x}_k) = \left[h_{j,\rho}^{(i)}(\mathbf{x}_k), h_{j,\theta}^{(i)}(\mathbf{x}_k), h_{j,d}^{(i)}(\mathbf{x}_k)\right]^{\mathrm{T}}$. The individual components are defined as

$$\begin{aligned}
h_{j,\rho}^{(i)}(\mathbf{x}_k) &= |\mathbf{p}_k - \mathbf{r}_i| + |\mathbf{p}_k - \mathbf{s}_j| \\
h_{j,\theta}^{(i)}(\mathbf{x}_k) &= \arctan\left(\frac{y_k - y_r^i}{x_k - x_r^i}\right) \\
h_{j,d}^{(i)}(\mathbf{x}_k) &= \frac{\mathbf{v}^{\mathrm{T}}}{2}\left[\frac{\mathbf{p}_k - \mathbf{r}_i}{|\mathbf{p}_k - \mathbf{r}_i|} + \frac{\mathbf{p}_k - \mathbf{s}_i}{|\mathbf{p}_k - \mathbf{s}_i|}\right].
\end{aligned}$$

Lastly, $\mathbf{w}_{j,\phi}^{(i)}$ is zero-mean Gaussian noise with a measurement error covariance of $\mathbf{R}_{j,\phi}^{(i)}$.

C. Measurement Simulation Environment

To generate realistic multistatic sonobuoy measurements, we use the Bistatic Range Independent Signal Excess (BRISE) simulation environment described in [20]. In brief, the environment works as follows: the target detection process is based on calculating a realization of the SNR for each target at each receiver. This SNR calculation employs precomputed signal excess component data, stored in look-up tables, that depend on the configuration of the sources and receivers, the waveform emitted and the target depth. Computation of the signal excess component data is carried out offline using the Gaussian ray bundle eigenray propagation model [21]. Using this SNR value, BRISE then decides whether a detection has occurred and, if so, it provides the measurement vector $\mathbf{z}$ corrupted by additive Gaussian measurement noise (the measurement covariances $\mathbf{R}_{j,\mathrm{CW}}^{(i)}$ and $\mathbf{R}_{j,\mathrm{FM}}^{(i)}$ of the noise are set in BRISE). False alarms are also generated using a Poisson distribution to determine the number of false detections and a uniform distribution from which to draw the elements of the measurement vector $\mathbf{z}$. Along with measurements BRISE also provides the probability of detection P_d^i, which is dependent upon the configuration of the sources and receivers, the waveform emitted and the depth of the target. For a complete review of the BRISE simulation environment see [7], [22].

D. Tracking Algorithm

Many algorithms have been proposed for tracking multiple underwater targets using a multistatic sonar field, for example see [23], [24]. In this paper, we opt for the robust multi-target multi-sensor Bernoulli tracker recently proposed in [22], [25]. The tracker combines the optimal Bayesian multi-sensor filter for a single target in clutter, also known as the multi-sensor Bernoulli filter [26]–[28], with the linear-multi-target paradigm [29]. This tracker uses the signal amplitude measurement associated with a detected target to discriminate between false alarms and tracks. It is also capable of processing measurements with different modalities (i.e. measurements from CW and FM waveforms). The tracker is designed using the Gaussian mixture model implementation outlined in [25].

In terms of the scheduling framework illustrated in Fig. 2, we obtain from the tracker a series of τ confirmed tracks. Each track comprises the current estimate of the target state $\hat{\mathbf{x}}_k$, the current error covariance $\mathbf{P}_k^{\tau}$ of the track, and the probability of existence for the track.

III. Sonobuoy Scheduling using Covariance-Based Cost Functions

At each transmission time, the scheduler must choose one action a from the following action space

$$\mathcal{A} = \mathcal{S} \times \mathcal{W} \tag{3}$$

where $\mathcal{S} = \{j_1, \ldots, j_{N_s}\}$ is the set of all sources, $\mathcal{W} = \{w_1, \ldots, w_{N_w}\}$ is the set of all waveforms and $\times$ represents the Cartesian product of the two sets. To make this choice, the scheduler requires a performance measure $\mathcal{J}$ to judge the relative merit, in terms of tracking performance, of each action. This measure acts as an objective function that can either be maximized or minimized in regards to a. In this paper, we propose the scheduling problem as a minimization of this objective function as follows:

$$\arg\min_a \ \mathcal{J}(a). \tag{4}$$

Accordingly, we refer to $\mathcal{J}(a)$ as the tracking cost function. Thus the scheduler functions by calculating this tracking cost for all actions in $\mathcal{A}$ and choosing the action with the smallest cost.

The question is therefore what cost function $\mathcal{J}$ should we use to ensure high quality tracking of a target? A suitable answer, commonly used in sensor management problems [15]–[17], is to formulate a cost based on the inverse of the *filtering* information matrix of the future tracker states – the predicted track error covariance matrix $\tilde{\mathbf{P}}$. It is this option that we shall now explore. Note that $\tilde{\mathbf{P}}$ is also referred to as the posterior[1] Cramér-Rao bound [13], [15] or Bayesian Cramér-Rao bound [30].

In the following, we shall use $\sim$ to indicate the predicted value of a variable and $\wedge$ to indicate its current estimated value.

[1]The use of 'posterior' indicates that the noise covariance $\mathbf{Q}$ is used when calculating the Cramér-Rao bound.

A. Predicted Track Error Covariance Matrix

The predicted track error covariance matrix $\tilde{\mathbf{P}}$ encapsulates how the error covariance of a track will be affected by both the addition of new measurement data and the future movement of the target. Specifically, measurements of the target should reduce the covariance whereas the uncertainty due to target movement has the opposite effect. Accordingly we use this matrix to measure the benefit of each action in $\mathcal{A}$.

To calculate this predicted covariance matrix, we use the recursive method proposed by Tichavsky *et al.* [13] to estimate the *filtering* information matrix and then take the inverse of the result. For a complete derivation of this method see [13] or, more recently, [31, Ch.4]. In this method the information matrix comprises two parts: the prior information matrix $\mathbf{J}_{\mathrm{p}}$, which describes the how the inverse of the current error covariance $\mathbf{P}_{k-1}$ propagates due to the motion model; and the measurement information matrix $\mathbf{J}_{\mathrm{m}}(a)$, which describes the gain in information from an action. Accordingly, for an action $a \in \mathcal{A}$, the predicted error covariance matrix for a single track at time k in the sonobuoy field is

$$\tilde{\mathbf{P}}(a) = \left[\mathbf{J}_{\mathrm{p}} + \sum_{i \in I_k(a)} \mathbf{J}_{\mathrm{m}}^{(i)}(a)\right]^{-1} \tag{5}$$

where $I_k(a)$ is the set of proximal receivers that will contribute measurements if action a is taken and $\mathbf{J}_{\mathrm{m}}^{(i)}(a)$ is the corresponding measurement information matrix for the ith receiver. The proximal set of receivers is defined geometrically as the group of receivers within a circle centred at the transmitting source with a radius twice that of the receiver-source separation.

The prior information matrix is obtained as follows:

$$\mathbf{J}_{\mathrm{p}} = \left[\mathbf{F}_{k-1}\mathbf{P}_{k-1}\mathbf{F}_{k-1}^{\mathrm{T}} + \mathbf{Q}\right]^{-1} \tag{6}$$

where $\mathbf{P}_{k-1}$ is the error covariance matrix for the track and $\mathbf{F}_{k-1}$ is the Jacobian of the function $f(\mathbf{x})$ evaluated at $\hat{\mathbf{x}}_{k-1}$, i.e.

$$\mathbf{F}_{k-1} = \nabla_{\mathbf{x}} f(\mathbf{x})|_{\mathbf{x}=\hat{\mathbf{x}}_{k-1}}.$$

Note that, based on the motion model in (1), $\mathbf{F}_{k-1}$ is invariant in both time and state space thus it is identical for all tracks.

Assuming $\tilde{\mathbf{x}}_k$ is the predicted future state of the target obtained from the motion model, the individual measurement information matrices from each receiver are approximated as

$$\mathbf{J}_{\mathrm{m}}^{(i)}(a) = P_d^i(a)\left[\mathbf{H}_k^i(a)\right]^{\mathrm{T}}\left[\mathbf{R}_a^{(i)}\right]^{-1}\mathbf{H}_k^i(a) \tag{7}$$

where $P_d^i(a)$ is the expected probability that receiver i will detect the target at $\tilde{\mathbf{x}}_k$ and $\mathbf{H}_k^i(a)$ is the 3×4 Jacobian of the function $\mathbf{h}_a^{(i)}(\mathbf{x})$ evaluated at $\tilde{\mathbf{x}}_k$, i.e.

$$\mathbf{H}_k^i(a) = \nabla_{\mathbf{x}} \mathbf{h}_a^{(i)}(\mathbf{x})\Big|_{\mathbf{x}=\tilde{\mathbf{x}}_k}.$$

Note that we use action a to define both the source j and the type of waveform ϕ it emits and, in the case of emitting a FM waveform, the third row of the matrix will be all zeros. For a discussion on the exact calculation of the individual measurement information matrices from each receiver we refer the reader to [32].

The expected probability of detection $P_d^i(a)$ is dependent on the target depth, which is unknown to the scheduler. To overcome this limitation, we use a conservative approach whereby we consider several depths, uniformly spaced in $z \in [z_{\min}, z_{\max}]$, compute the probability of detection for each depth and then use the minimum probability.

B. Measuring the Size of the Error Covariance

Having defined the predicted track error covariance above, we now require a measure (or cost) that quantifies 'the size of' this matrix. Our approach is to use the geometric representation of $\tilde{\mathbf{P}}(a)$ – it represents an error hyper-ellipsoid in the target state space. Thus, the size of the covariance $\tilde{\mathbf{P}}(a)$ can be quantified by measuring the size of the hyper-ellipsoid. Accordingly, the goal of the scheduler is to choose an action a that corresponds to the smallest hyper-ellipsoid.

Now, how best to measure the size of a nD hyper-ellipsoid? Assuming $\tilde{\mathbf{P}}(a) = \tilde{\mathbf{P}}_1(a)\tilde{\mathbf{P}}_1^{\mathrm{T}}(a)$ and that the eigenvalues of $\tilde{\mathbf{P}}_1(a)$ are $\lambda_1 \geq \lambda_2 \ldots \geq \lambda_n$, then four possible options were proposed in [33]. The first two options, commonly used in sensor management [15], [16], are the trace and the determinant. The trace of $\tilde{\mathbf{P}}_1(a)$ is the sum of its eigenvalues, which, in terms of geometry, represents the sum of the lengths of the axes of the hyper-ellipsoid. Thus we have the trace cost function:

$$\mathcal{J}_{\text{trace}}(a) = \text{tr}\left(\tilde{\mathbf{P}}_1(a)\right) = \sum_n \lambda_n. \tag{8}$$

This function equates to the arithmetic mean and measures the average variance of the state estimation associated with action a. In contrast, the determinant of $\tilde{\mathbf{P}}_1(a)$ is the product of the eigenvalues, which is proportional to the hyper-volume of the ellipsoid. Thus our second cost function is:

$$\mathcal{J}_{\text{det}}(a) = \det\left(\tilde{\mathbf{P}}_1(a)\right) = \prod_n \lambda_n. \tag{9}$$

This function equates to the geometric mean or generalized variance associated with action a.

Next, the third measure from [33] is the average precision, or harmonic mean, which equates to the following cost:

$$\mathcal{J}_{\text{prec}}(a) = \text{tr}\left(\tilde{\mathbf{P}}_1^{-1}(a)\right)^{-1} = \left(\sum_n \frac{1}{\lambda_n}\right)^{-1}. \tag{10}$$

This cost is dominated by the value of the smallest eigenvalue thus minimizing $\mathcal{J}_{\text{Prec}}(a)$, w.r.t a, is approximately equivalent to minimizing the smallest variance. In contrast, the fourth cost function is the maximum eigenvalue, which equate to the maximum length of the hyper-ellipsoid:

$$\mathcal{J}_{\max}(a) = \max_n \lambda_n = \lambda_1. \tag{11}$$

Thus, minimizing $\mathcal{J}_{\max}(a)$ is equivalent to choosing an action that minimizes the maximum variance in the state estimation.

In the following, we shall compare the performance of all four of the cost functions. Furthermore, we introduce a fifth cost that is similar to $\mathcal{J}_{\max}(a)$ but takes into account that $\tilde{\mathbf{P}}(a)$

combines both position and velocity information. Specifically, $\tilde{\mathbf{P}}(a)$ is a 4×4 matrix where two of its eigenvalues correspond to positional information and the other two correspond to velocity. Thus, our fifth cost is the product of the maximum positional eigenvalue and the maximum velocity eigenvalue. Accordingly, we have

$$\mathcal{J}_{\text{Joint}}(a) = \lambda_1\lambda_3, \tag{12}$$

where we assume λ_1 and λ_2 correspond to position and the other two eigenvalues correspond to velocity.

IV. Simulation Results

To evaluate the different covariance cost functions, we examine the performance of our scheduler when using each measure in (4) on the tracking scenario illustrated in Fig. 1. This scenario comprises a 4×4 grid of transmitter sonobuoys, spaced $15\,\text{km}$ apart, with a 5×5 grid of receiver sonobuoys, offset relative to the transmitters, and one target (in the bottom right of the grid) to track. The scenario lasts for 40 minutes with a transmission every minute. The target follows the constant velocity model defined in (1). The depth of the target is drawn randomly for each simulation from a uniform distribution ranging from a minimum depth of $10\,\text{m}$ and maximum of $100\,\text{m}$. To further explore the impact of the measures, we compare the performance when the target is moving at a speed of $8\,\text{knots}$ to that obtained when the target's speed is $14\,\text{knots}$. Note that for each cost we perform 600 Monte-Carlo simulations and that the scheduler uses a predefined sequence of actions, based on the search criteria in [8], until the target has been found.

We use two metrics to assess the performance of the scheduler when using each cost function: the position error and the velocity error. The position error is the Euclidean distance between positional components of the confirmed tracks and the target. Similarly, the velocity error is the equivalent for the velocity components. To avoid outliers caused by false tracks skewing performance, we only consider position errors that are less than $100\,\text{m}$. Note that the choice of performance measures used to evaluate estimation algorithms has been investigated in [34], [35].

The performance results for the scheduler using each cost function are shown in Fig. 3. Fig. 3(a) compares the mean velocity error for each performance measure and Fig. 3(b) shows the corresponding mean position errors. The performance when the target is moving at $8\,\text{knots}$ is indicated by the blue 'o' markers, whereas the red 'x' markers indicate the results when the target is moving at $14\,\text{knots}$. The error bars on each graph represent the 5^{th} and 95^{th} quantiles for the simulations. Note that the values shown in the graphs are averaged over both the whole scenario time and the number of Monte-Carlo simulations. The two metrics are then put on a single scatter plot in Fig. 3(c). To accompany this analysis, histograms of the waveforms transmitted during the simulations are shown in Fig. 4. The figure shows how the proportions of transmitted waveforms varies with the type of performance measure used by the scheduler and the speed of the target – Fig. 4(a) corresponds to a target speed of $8\,\text{knots}$ and Fig. 4(b) to a speed of $14\,\text{knots}$. Note that these figures do not include the waveforms used when initially searching for the target.

In terms of the overall performance of scheduler, the figures demonstrate that using CW waveforms more often improves the velocity accuracy of scheduler whereas using FM waveforms more often improves positional accuracy. This relationship is expected as CW waveforms return a Doppler estimate (i.e. movement information about the target). Similarly, increasing the target speed results in CW waveforms being chosen more often; again this is to be expected as the probability of detecting a target with CW increases with its speed.

Now, in terms of cost function choice, the figures show that the cost function has a clear effect on the type of waveform chosen by the scheduler, which in turn affects its performance. For example, regardless of target speed, when using $\mathcal{J}_{\text{prec}}$ as a cost function the scheduler chooses CW waveforms 98% of the time, which results in the smallest velocity error but the largest positional error. In contrast, the opposite performance is obtained when using either $\mathcal{J}_{\text{trace}}$ or $\mathcal{J}_{\text{max}}$ due to the scheduler only selecting FM waveforms. Sitting in between these two extremes are the $\mathcal{J}_{\text{det}}$ and $\mathcal{J}_{\text{joint}}$ cost functions. The histograms in Fig. 4 show that both functions result in the scheduler choosing a mixture of waveforms. For a target speed of $8\,\text{knots}$, the FM-CW mix is roughly 47%–53% using $\mathcal{J}_{\text{det}}$ and 69%–31% using $\mathcal{J}_{\text{joint}}$; the mixes for both costs change to 18%–82% when the target is moving at $14\,\text{knots}$. The greater use of CW by $\mathcal{J}_{\text{det}}$ again results in a lower velocity error compared to $\mathcal{J}_{\text{joint}}$ at the expense of the positional error. More precisely, for a target speed of $14\,\text{knots}$, Fig. 3(c) shows that the joint position-velocity performance obtained using each cost function is Pareto optimal [36], i.e. optimal in the sense that a lower velocity error cannot be obtained without degrading the position error and vice-versa. Similarly, for the slower target speed of $8\,\text{knots}$, the joint position-velocity performances of $\mathcal{J}_{\text{prec}}$, $\mathcal{J}_{\text{det}}$, $\mathcal{J}_{\text{joint}}$ and $\mathcal{J}_{\text{trace}}$ are also Pareto optimal. Accordingly, the choice of cost function is very important to the scheduler as it controls the trade-off between position and velocity error.

Finally, to complete this analysis, we include the histograms of the sources selected to transmit during the simulations when the target's speed is $14\,\text{knots}$. These histograms are shown in Fig. 5: Parts (a) to (e) show respectively the results for $\mathcal{J}_{\text{prec}}$, $\mathcal{J}_{\text{det}}$, $\mathcal{J}_{\text{joint}}$, $\mathcal{J}_{\text{trace}}$ and $\mathcal{J}_{\text{max}}$. Similarly to the waveform choice, each cost function chooses a slightly different mixture of sources during the simulations. In particular, $\mathcal{J}_{\text{trace}}$ and $\mathcal{J}_{\text{max}}$ make greater use of the source at location $(2,2)$ than the other cost functions. Note that we exclude the corresponding histograms for the slower target as the distance it travels during the scenario is relatively small resulting in the cost functions choosing very similar sources.

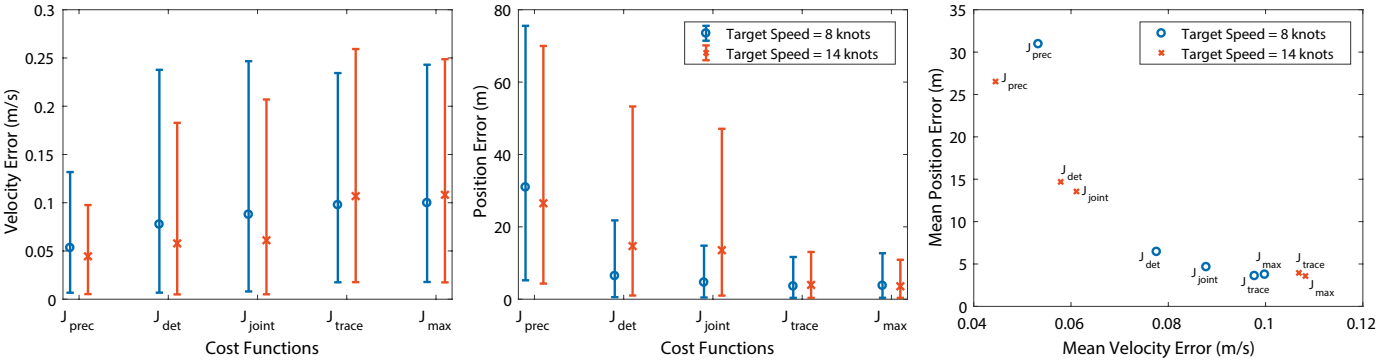

(a) Velocity Error (m/s) (b) Position Error (m) (c) Position vs Velocity Error Plot

Fig. 3. Performance of the scheduler. Part (a) shows the mean velocity error obtained using the different cost functions, part (b) shows the mean position error for the same costs and part (c) combines the means of both errors on a scatter. The blue lines (and 'o') indicate the performances when the target speed is 8 knots, and the red lines (and 'x') correspond to when the target speed is 14 knots. The markers represent the mean values and the error bars indicate the 5^{th} and 95^{th} quantiles.

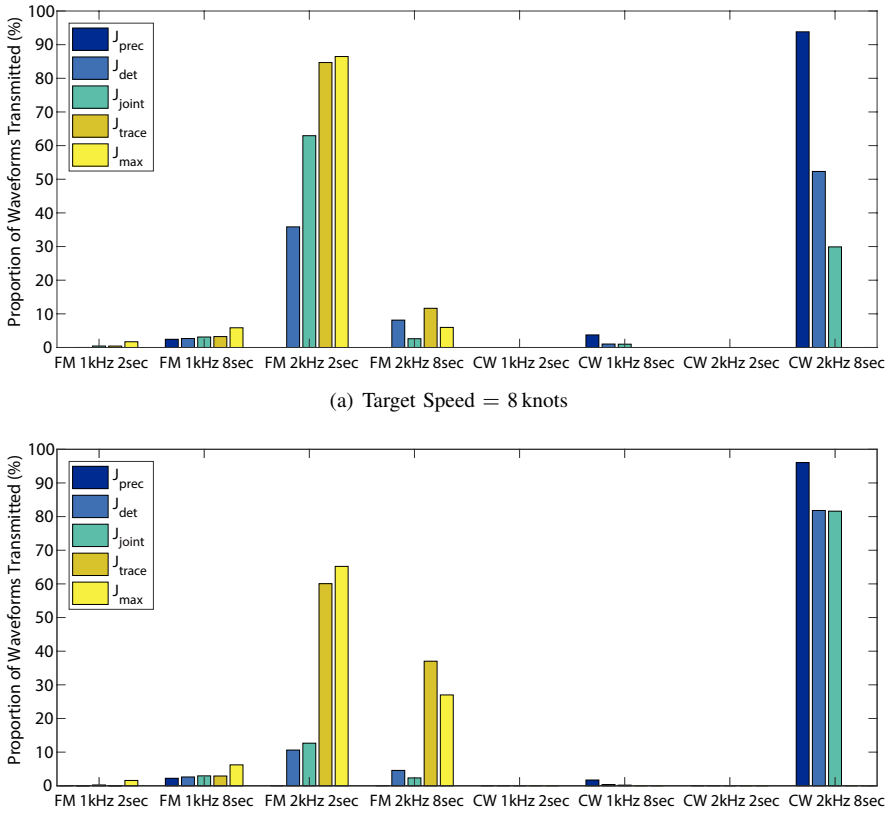

(a) Target Speed = 8 knots

(b) Target Speed = 14 knots

Fig. 4. Waveform histograms for the scenario illustrated in Fig. 1. The histograms show the proportion of waveforms transmitted when using each cost function to track the target. Part (a) shows the choice of waveforms used when the target's speed is 8 knots and part (b) shows the corresponding choice when the target's speed is 14 knots.

V. Conclusions

In this paper, we have presented a study on the choice of cost function when scheduling a multistatic sonobuoy field in a myopic fashion. Specifically, we have explored the effect of 5 different cost functions, derived from the predicted track error covariance matrix, on the scheduling performance. Based on interpreting the covariance as a hyper-ellipsoid, each cost represented a different measure of the size of the hyper-ellipsoid. Accordingly, the task of the scheduler is to decide the optimum source-waveform action that minimized the covariance cost function. Using a realistic measurement simulation environment, we demonstrated that the cost function choice affected the type of actions selected by the scheduler and thus affected its tracking performance. In particular, cost functions

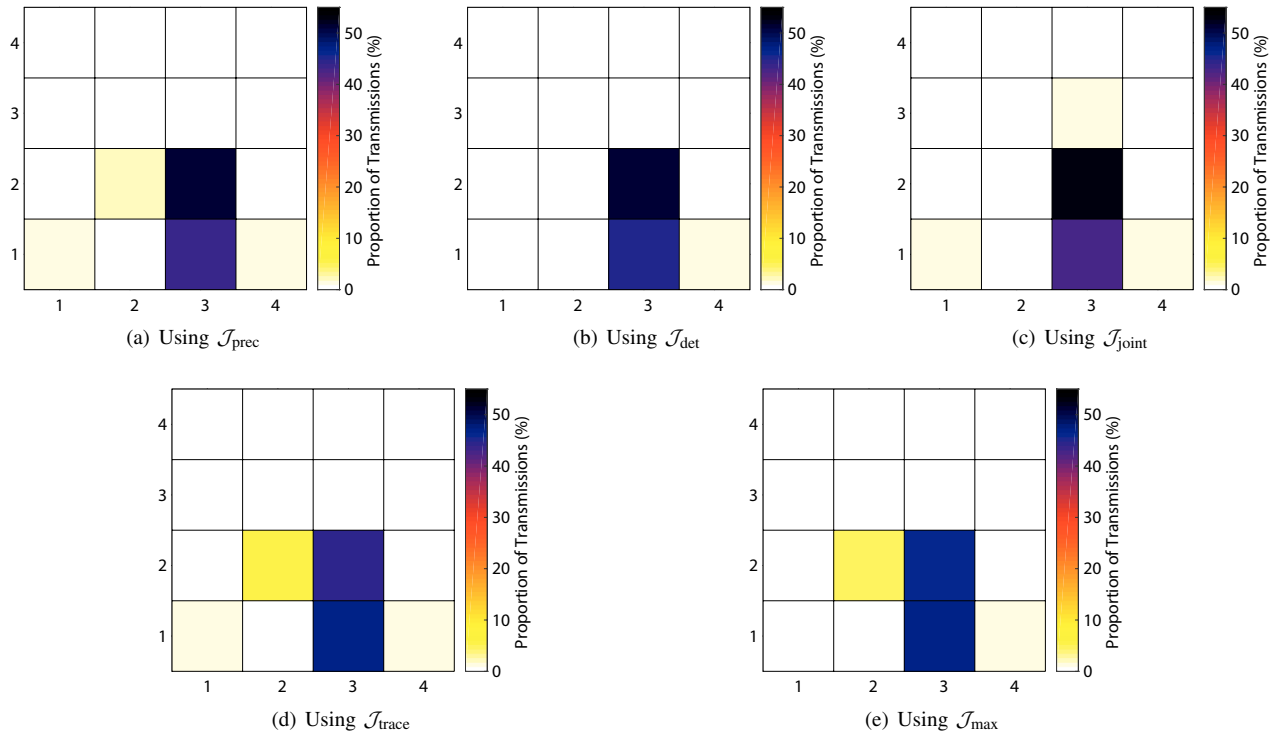

(a) Using $\mathcal{J}_{\text{prec}}$ (b) Using $\mathcal{J}_{\text{det}}$ (c) Using $\mathcal{J}_{\text{joint}}$

(d) Using $\mathcal{J}_{\text{trace}}$ (e) Using $\mathcal{J}_{\max}$

Fig. 5. Transmitter histograms for the scenario illustrated in Fig. 1 when the target's speed is 14 knots. The histograms show the proportion of transmissions from each source when using the different cost functions. Note that each cell represents a transmitter in the field and the grid orientation corresponds to the field geometry in Fig. 1.

that used more CW waveforms improved the scheduler's velocity estimation whereas use of FM waveforms improved its position estimation. Importantly, we showed that no one cost function is superior in terms of both position and velocity accuracy – there is a trade-off between the two. In fact, with only one exception, we found that the performance of our 5 cost functions in the position-velocity error space formed a set of Pareto optimal points, i.e. improving the estimation of one quantity degraded the estimation of the other. In future work, we intend to explore adaptively switching the cost function mid simulation in order to obtain the best of both worlds: good positional estimation and good velocity estimation.

References

[1] D. Krout, M. El-Sharkawi, W. Fox, and M. Hazen, "Intelligent ping sequencing for multistatic sonar systems," in *Proc. Int. Conf. Inf. Fusion (FUSION)*, Florence, Italy, 2006, pp. 1–6.

[2] D. Krout, W. Fox, and M. El-Sharkawi, "Probability of target presence for multistatic sonar ping sequencing," *IEEE J. Ocean. Eng.*, vol. 34, no. 4, pp. 603–609, 2009.

[3] B. I. Incze and S. Dasinger, "A Bayesian method for managing uncertainties relating to distributed multistatic sensor search," in *Proc. Int. Conf. Inf. Fusion (FUSION)*, Florence, Italy, 2006, pp. 1–7.

[4] S. Simakov and F. Fletcher, "GPU acceleration of threat map computation and application to selection of sonar field controls," in *Proc. Int. Conf. Acoust., Speech and Signal Process. (ICASSP)*, Brisbane, Australia, 2015, pp. 1827–1831.

[5] C. Y. Wakayama, D. J. Grimmett, and Z. B. Zabinsky, "Forecasting probability of target presence for ping control in multstatic sonar networks using detection and tracking models," in *Proc. Int. Conf. Inf. Fusion (FUSION)*, Chicago, IL, USA, 2011, pp. 1–8.

[6] C. Y. Wakayama and D. J. Grimmett, "Adaptive ping control for track-holding in multistatic active sonar networks," in *Proc. Int. Conf. Inf. Fusion (FUSION)*, Edinburgh, UK, 2010, pp. 1–8.

[7] S. Suvorova, M. Morelande, B. Moran, S. Simakov, and F. Fletcher, "Ping scheduling for multistatic sonar systems," in *Proc. Int. Conf. Inf. Fusion (FUSION)*, Salamanca, Spain, 2014, pp. 1–8.

[8] C. Gilliam, D. Angley, S. Suvorova, B. Ristic, B. Moran, F. Fletcher, H. Gaetjens, and S. Simakov, "Scheduling of multistatic sonobuoy fields using multi-objective optimization," in *Proc. Int. Conf. Acoust., Speech and Signal Process. (ICASSP)*, Calgary, Canada, 2018, pp. 3206–3210.

[9] A. Saksena and I. J. Wang, "Dynamic ping optimization for surveillance in multistatic sonar buoy networks with energy constraints," in *IEEE Conf. Decision Control*, Cancun, Mexico, 2008, pp. 1109–1114.

[10] C. Y. Wakayama, Z. B. Zabinsky, and D. J. Grimmett, "Linear optimization models with integer solutions for ping control problems in multistatic active acoustic networks," in *Proc. Int. Conf. Inf. Fusion (FUSION)*, Singapore, 2012, pp. 2354–2361.

[11] D. Angley, S. Suvorova, B. Ristic, W. Moran, F. Fletcher, H. Gaetjens, and S. Simakov, "Sensor scheduling for target tracking in large multistatic sonobuoy fields," in *Proc. Int. Conf. Acoust., Speech and Signal Process. (ICASSP)*, New Orleans, LA, USA, 2017, pp. 3146–3150.

[12] D. Angley, R. Ristic, S. Suvorova, B. Moran, F. Fletcher, H. Gaetjens, and S. Simakov, "Non-myopic sensor scheduling for multistatic sonobuoy fields," *IET Radar, Sonar & Navig.*, vol. 11, no. 12, pp. 1770–1775, 2017.

[13] P. Tichavsky, C. H. Muravchik, and A. Nehorai, "Posterior Cramér-Rao bounds for discrete-time nonlinear filtering," *IEEE Trans. Signal Process.*, vol. 46, no. 5, pp. 1386–1396, May 1998.

[14] M. Kalandros, "Covariance control for multisensor systems," *IEEE Trans. Aerosp. Electron. Syst.*, vol. 38, no. 4, pp. 1138–1157, 2002.

[15] M. L. Hernandez, T. Kirubarajan, and Y. Bar-Shalom, "Multisensor resource deployment using posterior Cramér-Rao bounds," *IEEE Trans. Aerosp. Electron. Syst.*, vol. 40, no. 2, pp. 399–416, 2004.

[16] C. Yang, L. Kaplan, and E. Blasch, "Performance measures of covariance and information matrices in resource management for target state

estimation," *IEEE Trans. Aerosp. Electron. Syst.*, vol. 48, no. 3, pp. 2594–2613, 2012.
[17] D. J. Kershaw and R. J. Evans, "Optimal waveform selection for tracking systems," *IEEE Trans. Inf. Theory*, vol. 40, no. 5, pp. 1536–1550, 1994.
[18] N. H. Nguyen, K. Dogancay, and L. M. Davis, "Adaptive waveform selection for multistatic target tracking," *IEEE Trans. Aerosp. Electron. Syst.*, vol. 51, no. 1, pp. 688–701, 2015.
[19] R. H. Hardin and N. J. A. Sloane, "A new approach to the construction of optimal designs," *J Statistical Planning and Inference*, vol. 37, no. 3, pp. 339–369, 1993.
[20] S. Simakov, "Signal excess data and tools for multistatic sonar emulation," Tech. Report DSTO-TR-3026, DSTO, 2014.
[21] H. Weinberg and R. E. Keenan, "Gaussian ray bundles for modeling high-frequency propagation loss under shallow-water conditions," *J. Acoust. Soc. America*, vol. 100, no. 3, pp. 1421–1431, 1996.
[22] B. Ristic, D. Angley, F. Fletcher, S. Simakov, H. Gaetjens, S. Suvorova, and B. Moran, "Bayesian multitarget tracker for multistatic sonobuoy systems," in *Proc. Int. Conf. Inf. Fusion (FUSION)*, Heidelberg, Germany, 2016, pp. 2171–2178.
[23] F. Fletcher and S. Arulampalam, "A comparison of existence-based multitarget trackers for multistatic sonar," in *Proc. Int. Conf. Inf. Fusion (FUSION)*, Singapore, 2012, pp. 2362–2369.
[24] J. Georgy, A. Noureldin, and G. R. Mellema, "Clustered mixture particle filter for underwater multitarget tracking in multistatic active sonobuoy systems," *IEEE Trans. Syst. Man Cybern. C, Appl. Rev.*, vol. 42, no. 4, pp. 547–560, 2012.
[25] B. Ristic, D. Angley, S. Suvorova, B. Moran, F. Fletcher, H. Gaetjens, and S. Simakov, "Gaussian mixture multitarget multisensor Bernoulli tracker for multistatic sonobuoy fields," *IET Radar, Sonar & Navig.*, vol. 11, no. 12, pp. 1790–1797, 2017.
[26] B. T. Vo, C. M. See, N. Ma, and W. T. Ng, "Multi-sensor joint detection and tracking with the Bernoulli filter," *IEEE Trans. Aerosp. Electron. Syst.*, vol. 48, no. 2, pp. 1385–1402, 2012.
[27] B. Ristic and A. Farina, "Target tracking via multi-static Doppler shifts," *IET Radar, Sonar & Navig.*, vol. 7, no. 5, pp. 508–516, 2013.
[28] B. Ristic, B. T. Vo, B. N. Vo, and A. Farina, "A tutorial on Bernoulli filters: Theory, implementation and applications," *IEEE Trans. Signal Process.*, vol. 61, no. 13, pp. 3406–3430, 2013.
[29] D. Mušicki and B. La Scala, "Multi-target tracking in clutter without measurement assignment," *IEEE Trans. Aerosp. Electron. Syst.*, vol. 44, no. 3, pp. 877–896, 2008.
[30] H. Van Trees and K. Bell, *Bayesian Bounds for Parameter Estimation and Nonlinear Filtering/Tracking*, Wiley-IEEE Press, 2007.
[31] B. Ristic, S. Arulampalam, and N. Gordon, "Beyond the Kalman filter: Particle filters for tracking applications," *Artech House*, 2004.
[32] M. Hernandez, A. Farina, and B. Ristic, "Posterior Cramér-Rao bounds for target tracking," in *Novel Radar Techniques and Applications Volume 2: Waveform Diversity and Cognitive Radar, and Target Tracking and Data Fusion*, R. Klemm *et al*, Ed., chapter 9, pp. 263–302. Institution of Engineering and Technology, 2017.
[33] M. Friendly, G. Monette, and J. Fox, "Elliptical insights: Understanding statistical methods through elliptical geometry," *Statistical Science*, vol. 28, no. 1, pp. 1–39, 2013.
[34] X.R. Li and Z. Zhao, "Evaluation of estimation algorithms part I: Incomprehensive measures of performance," *IEEE Trans. Aerosp. Electron. Syst.*, vol. 42, no. 4, pp. 1340–1358, October 2006.
[35] H. Yin, J. Lan, and X. Rong Li, "Measures for ranking estimation performance based on single or multiple performance metrics," in *Proc. Int. Conf. Inf. Fusion (FUSION)*, Istanbul, Turkey, 2013, pp. 453–460.
[36] V. Pareto, "Manuale di economica politica, societa editrice libraria," *Manual of political economy*, vol. 1971, 1906.